

Self-assembly in Mixtures of Charged Lobed Particles

Arpita Srivastava, 1,† Brunno C. Rocha, 1,† and Harish Vashisth 1,*

¹Department of Chemical Engineering, University of New Hampshire, 33 Academic Way, Durham, NH 03824, USA

†equal contribution

Correspondence*:
Harish Vashisth
harish.vashisth@unh.edu

2 ABSTRACT

- 3 We report coarse-grained Langevin dynamics simulations of homogeneous mixtures of lobed
- 4 colloidal particles with opposite charges. We show that dumbbell, trigonal planar, tetrahedral,
- square planar, trigonal bipyramidal, and octahedral shaped particles form distinct self-assemblies
- 6 including chains, sheets, crystalline, and spherical structures. The dumbbell and square planar
- 7 particles predominantly form chains and sheets while other particles form network-like self-
- 8 assembled morphologies. At higher temperatures and lower charges, non-planar particles form
- 9 three-dimensional aggregates. We further report on packing arrangements of particles which
- lead to differences in porosities within self-assembled morphologies. Our results show that the
- 11 trigonal planar particles form larger porous structures. The self-assembled structures that we
- 12 report are potentially useful in designing porous biomaterials for biomedical applications.
- 13 Keywords: self-assembly, charged lobed particles, particle mixtures, porous structures

1 INTRODUCTION

14 Self-assembly is an approach where the components of a system spontaneously assemble without the

15 application of external forces [1, 2]. The self-assembled structure gains its stability from the interactions

among its constituents. Colloidal particles are one such class of materials which have been widely studied for

17 their tendency to form larger clusters with distinct morphologies [3, 4, 5]. The interactions of significance in

8 these assemblies include van der Waals interactions (vdW) [6], electrostatic interactions [7], steric effects,

19 [8] and solvation forces [9, 10]. Colloidal systems have served as models in understanding fundamental

20 and applied problems including phase behavior [11], glass transition [12, 13], crystal nucleation [14, 15],

21 and biomedical applications [16, 17, 18].

22 Self-assemblies of patchy colloidal particles are known for their distinct shapes and novel applications

23 [19, 20, 21, 22]. The placement of patches on colloidal particles leads to selective and tunable interactions

24 that allow control over the morphologies of the structures formed via self-assembly [23, 24]. These

patches can take the form of lobes that protrude from the surface of colloidal particles. As a result, the

lobes can dictate the phase behavior and porosity of a given self-assembled structure due to their size,

27 number, location, and inter-particle interactions, in addition to environmental conditions [25]. Our previous

28 simulation studies have shown that the incorporation of lobes in colloidal particles results in the formation

29 of structures with enhanced porosity due to an increase in the excluded volume created by the non-spherical

30 shapes of particles [18, 25, 26, 27].

25

26

33

34

35

37

44

31 Interest in the synthesis and self-assembly of colloidal particles with lobes has been increasing in recent

32 years [28, 29, 30, 31, 32, 33, 34, 35, 36, 37, 38]. A pioneering study by Wang et al. [29] reported the

synthesis of colloidal particles with lobes in positions that mimic hybridized atomic orbitals, which provide

three-dimensional bonding symmetries that may give rise to novel self-assembled structures. Liu and

colleagues [30] have synthesized dumbbell-shaped particles and observed that when the particle lobes

36 are DNA-coated, these particles self-assemble to form Kagome lattices, brick-wall-like lattices, or a co-

existence of these two arrangements, based on the temperature of the system. Wolters et al. [37] synthesized

38 two-lobed particles with a "Mickey Mouse" shape and reported that these particles self-assemble to form

39 tube-like structures.

40 Simulations have been systematically conducted for studying the assemblies of tri-block patchy colloidal

41 particles of tetrahedral and octahedral shapes which result in the formation of colloidal crystals of body

42 centered cubic and cubic diamonds [39]. Simulations of dumbbell-shaped particles show the formation

43 of micelles, vesicles or bilayers with a change in size ratio, separation between two dumbbell spheres

and volume fraction [40]. Further, using experimental and computational approaches, dumbbell-shaped

45 particles were shown to stabilize microspheres against aggregation[41]. Simulations of spherical patchy

particles have highlighted the dependence of the interaction strength, patch coverage, and density as the key factors in forming two-dimensional self-assemblies [42, 43]. However, lobed patchy particles and their

mixtures have been underexplored for the creation of porous colloidal self-assemblies.

We have previously reported simulation studies on the self-assembly of lobed colloidal particles [18, 49 50 25, 26, 27, 44]. We considered different particle types, as in the current work (dumbbell, trigonal planar, square planar, tetrahedral, trigonal bipyramidal, and octahedral), and investigated their morphologies 51 and porosities where the lobes of these particles are either neutral, charged, or functionalized. Many of 52 these particle types have been successfully designed using experimental approaches, thereby highlighting 53 the feasibility of creating larger lobes instead of patches [45, 46, 47, 48, 49]. However, in one of our 54 previous studies in which the lobed particles with charges were studied [27], the positive and the negative 55 charges are placed on different lobes of the same particle to have a net charge of zero on the particle, but 56 experimentally designing lobed particles where different lobes on the same particle can be functionalized 57 differently is significantly challenging. In contrast, it is conceivable that all lobes on a given particle can be 58 functionalized uniformly to have complementary interactions between a pair of distinctly-functionalized 59 60 particles.

In this work, we introduce a new design of lobed colloidal particles with uniformly-charged lobes where we assign either an overall positive or an overall negative charge to all lobes of a given type of particle (Fig. 1) to mimic complementary interactions between the lobes. For observing self-assembly due to complementary interactions, we study 1:1 mixtures of the same type of particle where half of the particles in the mixture have positively-charged lobes and the other half have negatively-charged lobes, thus studying an overall electrically neutral system. Along with investigating the role of the particle design, charges, and temperature on the phase behavior and porosity, we also focus on packing modes of particles which lead to differences in porosities of the self-assembled structures.

2 MODELS AND METHODS

69 2.1 Model

We conducted Langevin molecular dynamics simulations to study the self-assembly behavior of six different types of lobed particles with oppositely-charged lobes. These particles with distinct shapes include dumbbell (S_2^{DB}) , trigonal planar (S_3^{TP}) , square planar (S_4^{SP}) , tetrahedral (S_4^{TH}) , trigonal bipyramidal (S_5^{TB}) , and octahedral (S_6^{OC}) particles. We prepared six different homogeneous systems by mixing particles of the same type but with opposite charges on the lobes (Fig. 1). We used a seed (σ_S) to lobe (σ_L) diameter ratio of 2:1, respectively, with their masses $(m_S$ and $m_L)$ set as 1. The mixed system is prepared with the lobes on half of the particles having positive charges and on the remaining half of the particles having negative charges of equal magnitudes, thus, making an overall neutral system. Consistent with our previous

82

83

84

85

86

study [27], we used charges on the lobes with magnitudes of 2, 4 and 6 units for each type of particle. We utilized reduced units for all parameters used in our simulations and used harmonic potentials to maintain the shape of the particles during simulations, as described in our previous studies [18, 25, 26, 27, 44].

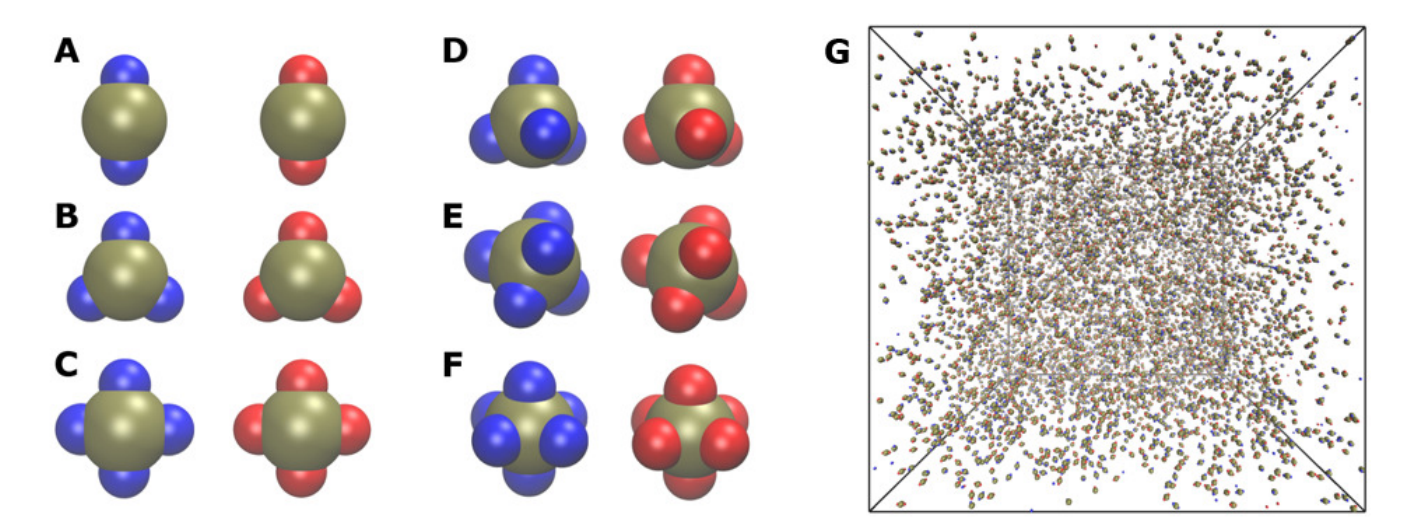


Figure 1. Snapshots of particle geometries studied in this work: (A) Dumbbell (S_2^{DB}) , (B) Trigonal planar (S_3^{TP}) , (C) Square Planar (S_4^{SP}) , (D) Tetrahedral (S_4^{TH}) , (E) Trigonal bipyramidal (S_5^{TB}) , and (F) Octahedral (S_6^{OC}) . The seeds are colored tan, the positively-charged lobes are colored blue, and the negatively-charged lobes are colored red. Two representations of each particle in the panels A-F indicate that a 1:1 mixture of the same type of particles was studied. (G) A snapshot of the simulation domain showing a typical randomized initial configuration.

2.2 Non-bonded and electrostatic interactions

The self-assembly of charged colloidal particles is mediated by short-range interactions as well as long-range electrostatic interactions [50]. The model used in our simulations accounts for both types of interactions. The seed-seed (S-S), lobe-lobe (L-L), and seed-lobe (S-L) non-bonded interactions are modeled by using the shifted Lennard-Jones (SLJ) potential (Equation 1). The SLJ potential was chosen to model the non-bonded interactions because the diameters of the colloidal particles of interest are in the μ m range. Therefore, the interactions are computed between the surfaces of the particles rather than between the centers of the particles [51].

$$U_{SLJ}(r_{ij}) = 4\epsilon_{ij} \left[\left(\frac{\sigma}{r_{ij} - \delta} \right)^{12} - \left(\frac{\sigma}{r_{ij} - \delta} \right)^{6} \right]$$
 (1)

In this equation, ϵ_{ij} denotes the depth of the potential well for a pair of particles i and j and σ denotes the distance of the closest approach. The equation is used to model the pairwise interaction potentials when $r_{ij} < r_{cut} + \delta$. Here, r_{cut} signifies a cut-off distance and $\delta = (\sigma_i + \sigma_j)/2 - 1$, where σ_i and σ_j are the particle diameters. When $r_{ij} \ge (r_{cut} + \delta)$, non-bonded interactions are neglected, i.e., $U_{SLJ}(r_{ij}) = 0$. The

depth of the pair-potential well for interactions between the positive and negative lobes is fixed as 3 in reduced units, while it was kept as 1 for all other pairs, similar to our previous work on particles with charges on the lobes [27]. The short-ranged repulsions are treated by setting the cut-off distance (r_{cut}) as $2^{\frac{1}{6}}\sigma$ in the SLJ potential for all pairs other than the negative lobe-positive lobe pairs, where an r_{cut} of 2.5σ is used to account for attractive interactions [51, 52, 53, 54, 55]. The σ values in the SLJ potential are set to 2.0, 1.5, and 1.0 for the seed-seed, seed-lobe and lobe-lobe interactions, respectively. The electrostatic interactions are computed with the following equation, using a cut-off of $15\sigma_L$ [56],

$$U_{Elec}(r_{ij}) = \frac{q_i q_j}{4\pi\epsilon_0 \epsilon_r} \frac{1}{r_{ij}} \tag{2}$$

where, q_i and q_j are charges on a pair of particles i and j, respectively, ϵ_0 is the 101 permittivity of the free space, and ϵ_r the relative permittivity. For electrostatic screening, 102 ϵ_r represents the dielectric permittivity of bulk water at ambient conditions (equal to 80).

2.3 Simulation details

103

104

105 We conducted coarse-grained Langevin dynamics simulations for all systems using the HOOMD-Blue software [57]. We computed the electrostatic interactions by using the particle-particle-mesh 106 107 (PPPM) method [58, 59]. Each system is composed of 8000 particles of the same type (4000 each with positively-charged and negatively-charged lobes, respectively) and the length of the simulation domain 108 is $160\sigma_L$ along each direction in all simulations. Overall, we simulated 6 distinct systems, each at 4 distinct temperatures and 3 distinct charge values. Specifically, we performed simulations of all six types 110 of particles at four different temperature conditions ($k_BT = 0.1, 0.4, 0.7, \text{ and } 1.0, \text{ in reduced units}$) with 111 three different magnitudes for the charges on the lobes (± 2 , ± 4 , and ± 6 in reduced units). We note that $k_BT=1.0$ corresponds to T = 298 K [60]. Therefore, k_BT = 0.1, 0.4, and 0.7 correspond to 29.8 K, 119.2 114 K, and 208.6 K, respectively.

We generated initial conditions for different systems by simulating for 10,000 steps at $k_BT=3.0$, a 115 sufficiently higher temperature to prevent any self-assembly at all conditions and to randomize the initial 116 configurations (Fig. 1G). In all simulations, we used an integration time-step of 0.005 and a simulation 117 length of 5×10^7 steps to equilibrate each system. We confirmed the stability of a given self-assembled 118 structure by analyzing the convergence of the potential energy per particle and the total number of clusters 119 (Fig. S1) as a function of the number of time-steps. The self-assembled clusters are formed by those 120 particles whose centers of masses are within $3.25\sigma_L$ from each other. The cluster calculation was carried 121 out using the freud software [61]. 122

2.4 Pore diameter and Interplanar angle measurements

We analyzed two types of pores in our self-assembled morphologies, the interstitial (Fig. 2A) and the intra-network pores (Fig. 2B). The interstitial pores arise in the system due to the formation of large three-dimensional self-assembled morphologies. The available spaces within these aggregates correspond to interstitial pores. The interstitial pore size is calculated by carving out a cube from a three-dimensional aggregate and the pores within the cube (zoomed view in Fig. 2A) are characterized as representative of the self-assembled morphology. The intra-network pores exist due to the formation of interconnected structures (chains, sheets and random aggregates) within the simulation domain. We consider the entire simulation domain for capturing the sizes of intra-network pores formed from different building blocks. We used the Zeo++ software [62, 63, 64] to compute the pore size diameter by measuring the diameter of the largest free sphere (D_{LFS}) which can freely diffuse through a self-assembled porous structure. For this, we considered a probe radius equivalent to $\frac{1}{2}\sigma_L$, similar to our previous work [18, 25, 26, 27, 44].

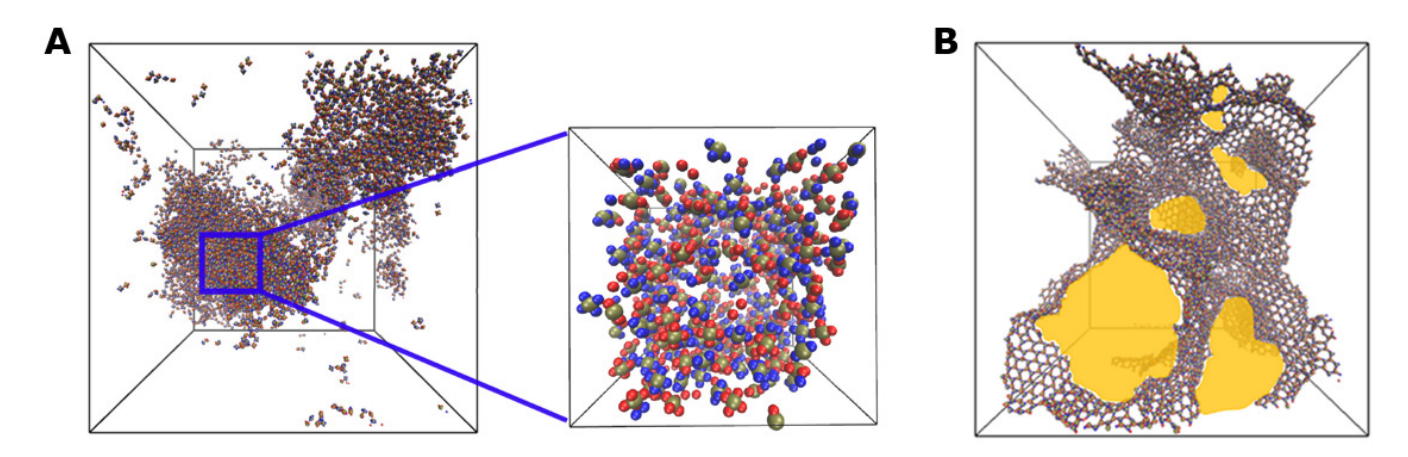


Figure 2. (A) A snapshot highlighting interstitial pores formed in three-dimensional aggregates. The zoomed-view shows a cube carved out of larger aggregates and used in the calculation of the sizes of interstitial pores. (B) A snapshot highlighting the intra-network pores (yellow) observed in self-assembled structures.

To characterize the packing arrangements among particles in self-assembled morphologies, we also computed the distributions of the interplanar angles between the planes formed by $S-L^+-L^-$ and L^+-L^- and L^- group of particles, where L^+ and L^- denote the positively-charged and negatively-charged lobes, respectively, and S signifies the central seed particle on which the lobes are placed. The interplanar angle values span the range between -180° and +180° which correspond to the interior/exterior angles between the two planes.

3 RESULTS AND DISCUSSION

We studied the self-assembly for six different types of lobed particles which differ in the number of lobes (Fig. 1) as well as their positions and charges. We systematically studied the effect of temperature

 $(k_BT=0.1, 0.4, 0.7, \text{ and } 1.0)$ and charges (2, 4, or 6 units) on the lobes with a focus on homogeneous mixtures of particles where half of the particles have positively-charged lobes and the remaining half have negatively-charged lobes. The time-evolution of the potential energy per particle and the total number of clusters in each system for a given condition of q and k_BT are shown in Fig. S1. Similar convergence trends were observed for all systems. Nonetheless, we note that patchy interactions may lead to the formation of kinetically trapped structures [65, 66, 67], especially at lower temperatures, and alternate methodologies [68, 69] could be explored in future studies to further probe such structures.

3.1 Self-assembled Morphologies

We analyzed the final configurations obtained at the end of the simulations for each system according to their morphologies. In Fig. 3, we summarize the phase behavior of different morphologies formed by these mixtures under all temperature and charge conditions.

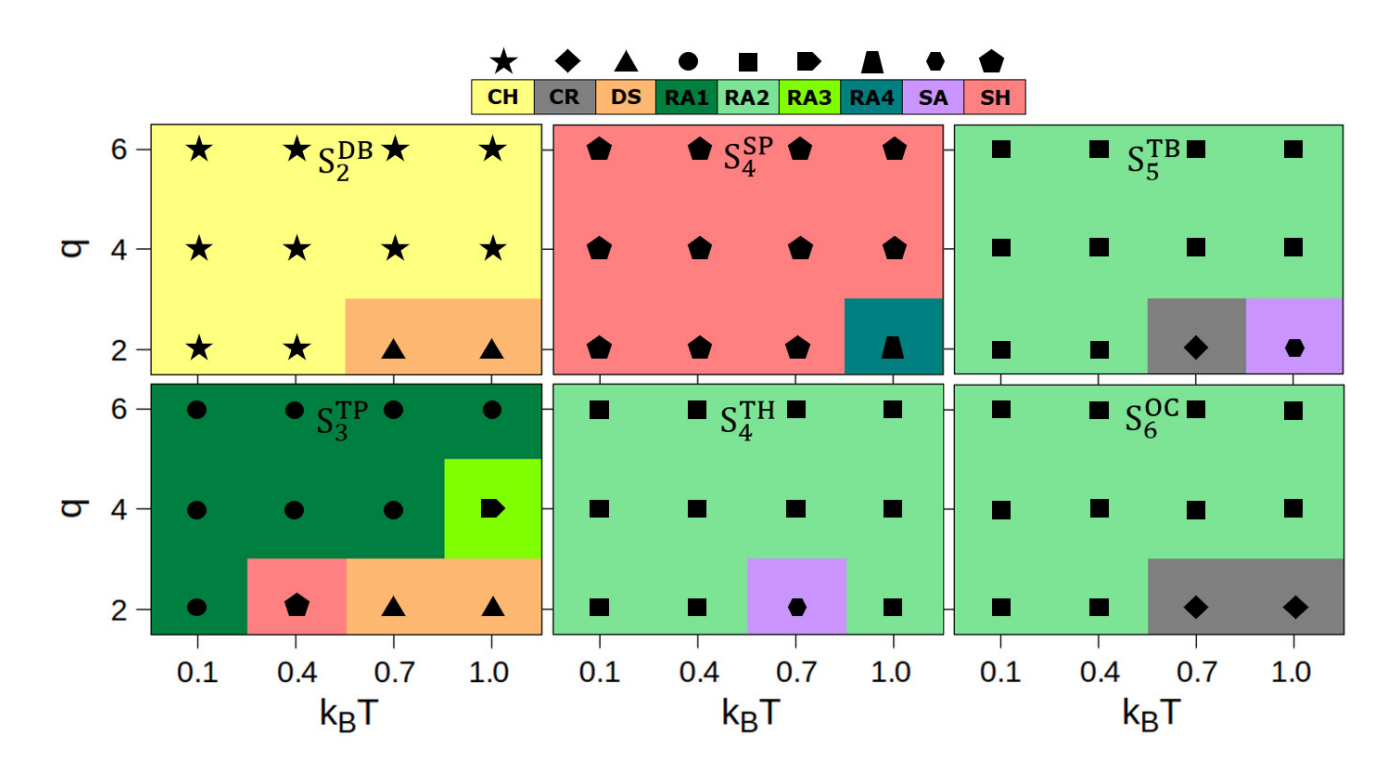


Figure 3. Phase behavior in homogeneous mixtures of charged lobed particles at all charge (q) and temperature (k_BT) conditions. Each type of morphology is color coded: chains (CH), crystalline self-assemblies (CR), random aggregates (RA1, RA2, RA3, RA4), sheets (SH), and spherical aggregates (SR). The conditions at which self-assembly is not observed are labeled as DS, the dissociated state.

These data reveal the formation of various types of network-like particle assemblies including chains (CH), different types of random aggregates (RA1, RA2, RA3, RA4), and two-dimensional sheets (SH), or three-dimensional clusters including crystalline (CR) and spherical aggregates (SA). The random aggregates termed RA1 and RA3 are formed by the planar particles (S_3^{TP}) with RA3 having the maximum porosity,

- RA2 are formed by the non-planar particles $(S_4^{TH}, S_5^{TB}, S_6^{OC})$, and RA4 are formed by the square planar
- 160 (S_4^{SP}) particles. At some conditions $(q = 2; k_BT = 0.7 \text{ and } 1.0), S_2^{DB}$ and S_3^{TP} particles do not form any
- 161 type of self-assembled structure, thereby remaining in a dissociated state (DS).
- 162 The relative occurrence of distinct phases in simulations of charged particles without mixing, as reported
- in our previous work [27], and homogeneous mixtures of charged particles from this work is shown in
- 164 Fig. S2 (magenta bars, previous work; green bars, this work). The fractional occurrence (expressed as a
- percentage) is computed by comparing the formation of a specific phase with respect to the total number of
- 166 phases formed in simulations. The homogeneous mixtures reported in this work have higher occurrences of
- some (CH, CR, RA1, RA2, and RA3) morphologies, and comparable occurrences of other (SA and SH)
- 168 morphologies. The RA4 morphology is only observed in homogeneous mixtures albeit at a significantly
- 169 lower fraction compared to other morphologies.

3.2 Structural Motifs in Self-assembled Morphologies

- For dumbbell-shaped particles with two lobes (S_2^{DB}) , at most conditions of charges and temperatures, we
- 173 observed the formation of linear chain-like (CH) arrangements (Fig. 4A) that originate from the electrostatic
- interactions between the oppositely-charged lobes. However, at a lower charge (q = 2), the electrostatic
- interactions are weaker at higher temperatures ($k_BT = 0.7$ and 1.0), where only a dissociated state (DS) is
- observed. The linear shape of dumbbell-shaped particles accounts for the formation of extended chain-like
- 177 (CH) networks. A zoomed view of these chains shows further chain coiling (highlighted in zoomed blue
- 178 circles, Fig. 4A), which leads to the formation of extended porous networks inside the simulation domain.
- 179 The oppositely-charged lobes of a pair of particles in different chains can attract each other via electrostatic
- 180 interactions causing elongated chain associations. In our previous study on functionalized lobed particles
- 181 [18], the S_2^{DB} particles also formed the CH phase. However, the overall morphology is different (Fig.
- 182 S3) in comparison to the current configuration (Fig. 4A). For example, only shorter chains without any
- 183 extended network and non-porous self-assembled morphologies were observed in our previous work [18].
- As the number of lobes increases, as in the case of S_3^{TP} particles, network-like assemblies arise from
- 185 random aggregates (RA1 or RA3) or sheet-like (SH) morphologies. In Figs. 4B, C and S4A, we show
- 186 self-assemblies formed by S_3^{TP} particles and the zoomed-views of the network-like morphology showing
- 187 cylindrical organization of particles. We classify this network-like organization assisted by two-dimensional
- sheets and three-dimensional particle arrangements as RA1. These kind of aggregates are predominantly
- observed in self-assemblies of S_3^{TP} particles, and can be attributed to the existence of an additional lobe
- 190 on the S_3^{TP} particles in comparison to the S_2^{DB} particles. In sheet-like morphologies formed by the S_3^{TP}
- 191 particles, we observed the formation of six-membered rings (Fig. 5A) in which the oppositely-charged lobes

193

194

195

197

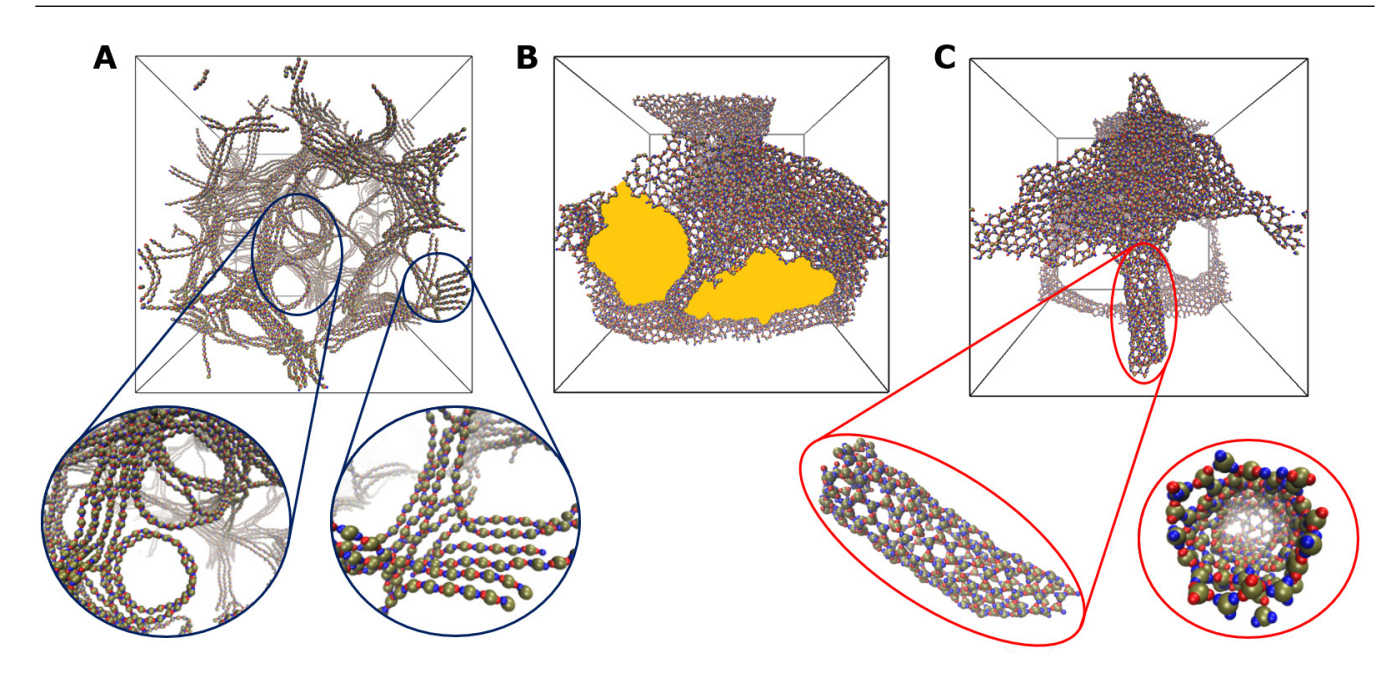


Figure 4. Snapshots highlighting self-assembled networks formed by the particles with two (S_2^{DB}) or three (S_3^{TP}) lobes. (A) Interconnected chain-like morphologies formed by the S_2^{DB} particles; and (B and C) random aggregates and hollow cylindrical morphologies formed by the S_3^{TP} particles. The blue and red circles show zoomed-in views, and a yellow patch (panel B) represents intra-network pore space.

interact via electrostatic interactions to form a network (Fig. S4A). This six-membered ring-like ("Kagome-lattice" type) arrangement is not present in our previous work on charged particles [27], where the existence of oppositely-charged lobes present on the same particle led to the formation of three-membered rings (Fig. 5B and S4B). Similarly, our previous work on self-assemblies formed by uncharged but functionalized lobes of S_3^{TP} particles favor the formation of honeycomb-like sheets with five or seven membered rings (Fig. 5C).

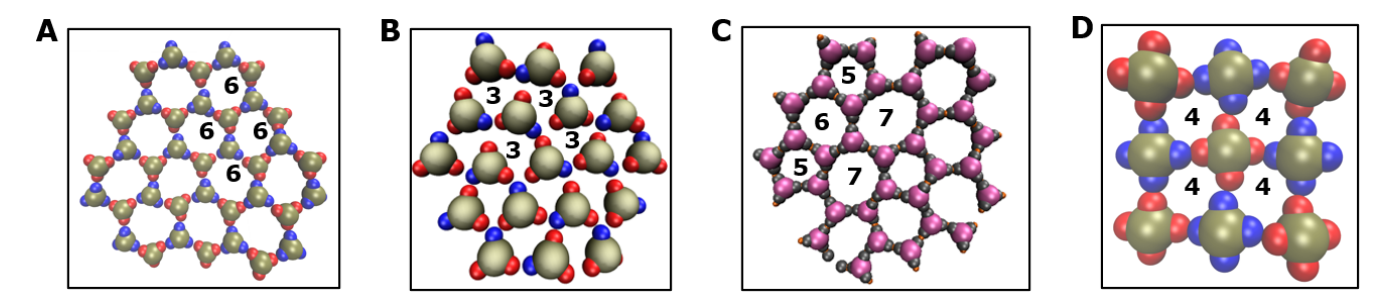


Figure 5. A comparison of structural motifs in sheet-like morphologies reported in this study and our previous work [18, 27]. (A, B, C) Ring-like arrangements of particles with three lobes are shown: 6 membered rings (panel A, current work), 3 membered rings (panel B, previous work [27]), and 5 or 7 membered rings (panel C, previous work [18]). (D) Four membered rings formed by square planar (S_4^{SP}) particles from our current work.

In Fig. S5, we show the systematic evolution of morphologies formed by S_3^{TP} particles from the current work, where the particles are initially randomly oriented within the simulation domain (Fig. S5A) but

- 200 gradually reorganize and self-assemble into three-dimensional networks (Fig. S5B-D) made up of ring-like
- 201 motifs (Fig. 5A). At a lower charge and higher temperature (q = 2 at $k_BT = 0.7$ or 1.0), we do not observe
- 202 self-assemblies due to higher thermal energies in comparison to electrostatic interactions, but at a moderate
- 203 charge but similar temperature (q = 4, $k_BT = 1.0$), we observed porous networks with larger intra-network
- 204 pores (highlighted by a yellow patch in Fig. 4B).
- Further, the particles with four lobes either have a square-planar (S_4^{SP}) or a tetrahedral (S_4^{TH}) geometry
- 206 (Fig. 1C-D). Due to the planar geometry of the S_A^{SP} particles, they predominantly self-assembled into
- 207 sheet-like (SH) morphologies (Fig. 3). The two oppositely-charged lobes on these particles act as the
- 208 connecting units responsible for a well-packed sheet-like structure where the inter-particle interaction form
- 209 a four-membered ring-like structural motif (Fig. 5D). This packing behavior of the S_A^{SP} particles is similar
- 210 to the one observed in our previous work [27]. At certain charge/temperature conditions (at q = 2, and $k_B T$
- 211 = 1.0), we also observed the formation of three-dimensional random aggregates (termed RA4) that do not
- 212 form an interconnected network of pores, but exist as three-dimensional clusters of random shapes. The
- 213 available pore spaces in these self-assembled morphologies serve as interstitial pores (Fig. 2A).
- In contrast, the S_4^{TH} particles having non-planar tetrahedral arrangement of four lobes do not form sheet-
- 215 like configurations but form network-like assemblies originating from random interconnected networks
- 216 (e.g., at q = 4 and 6; all T values; Fig. 3). We classify these network-like assemblies from randomly
- 217 organized particles as RA2. However, at a lower charge (q = 2), we identified the formation of spherical
- 218 aggregates (SA) at $k_BT = 0.7$, which transition into random network-like assemblies (RA2-type) at a
- 219 higher temperature ($k_BT = 1.0$) (Fig. S6).
- 220 Similar network-like morphologies originating from the RA2-type configurations are found in the
- assemblies of lobed particles with 5 or 6 lobes (S_5^{TB} and S_6^{OC}) at all temperatures (e.g., at q = 4 or 6 and
- 222 all T values; Fig. 3). Additionally, S_5^{TB} particles also form spherical aggregates ($q=2,\,k_BT=1.0$; Fig. 3),
- 223 and both types of particles form crystalline morphologies (q = 2, $k_BT = 0.7$; Fig. 3). In Fig. 6, we show the
- shape transitions among various morphologies for the S_5^{TB} particles, where network-like configurations
- 225 first switch to crystalline and then to spherical morphologies as temperature gradually increases (k_BT =
- 226 0.4, 0.7, and 1.0). This morphological transition is similar to the one observed in our previous study [27],
- 227 where the S_6^{OC} particles were observed to transition from random aggregates to crystalline structures and
- 228 further to spherical aggregates with a temperature change from $k_BT = 0.7$ to 1.1. These transitions occur
- 229 due to an intricate balance between the electrostatic interactions and thermal diffusive effects.

3.3 Interstitial and Intra-network Pore Sizes

230

- To probe the porosity of a given self-assembled structure, we computed the pore sizes (measured using
- 232 the diameter of the largest free sphere D_{LFS} as a metric) for all the assemblies at all conditions of charges

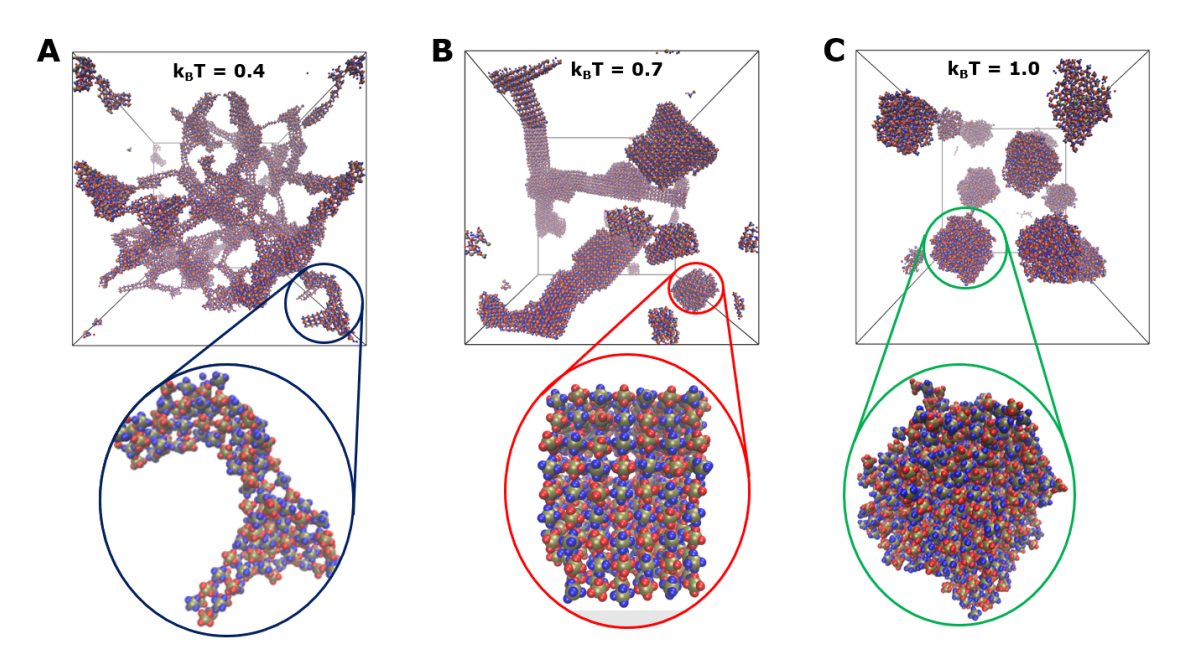


Figure 6. Shown are the snapshots highlighting temperature-dependent shape transitions in self-assemblies formed by the S_5^{TB} particles: (A) porous network-like assemblies; (B) crystalline morphologies; and (C) spherical aggregates.

and temperatures (Fig. S7). This analysis considered all particle shapes and the conditions responsible for the formation of pores of various diameters. The smaller pores originate from the interstitial space between particles in three-dimensional aggregates, while the larger pores originate from the intra-network void space in a given network-like morphology. Among all charge (q) values and temperatures, the pore-sizes with larger diameters are observed for q = 4, $k_B T = 0.7$ and 1.0.

In Fig. 7, we show the trends in pore sizes (D_{LFS}) for both interstitial and intra-network pores for self-assemblies formed by particles with 3 or more lobes $(S_3^{TP}, S_4^{SP}, S_4^{TH}, S_5^{TB}, S_6^{OC})$. The intra-network pores are an order of magnitude larger than the interstitial pores. For comparison, we also show the data from our previous study on charged lobed particles without mixtures [27] (magenta bars in Fig. 7) along with the data from our current study where mixtures are studied (green/cyan bars in Fig. 7). These data show that the interstitial pores are significantly larger in self-assemblies observed for S_4^{SP} , S_5^{TB} , and S_6^{OC} particles studied in our current work (Fig. 7A). This is attributed to larger porous sheets formed by the S_4^{SP} particles (Fig. 5D) or RA2-type random aggregates, crystalline, and spherical self-assembled morphologies formed by S_5^{TB} and S_6^{OC} particles. However, for self-assemblies formed by the S_4^{TH} particles in our current work, we observed smaller interstitial pores in comparison to our previous study [27] indicating a tighter packing of particles in random and spherical aggregates formed by them.

On comparing intra-network pores (Fig. 7B), we find that the network-like self-assemblies formed by particle mixtures studied in our current work have larger pores in most cases except for the

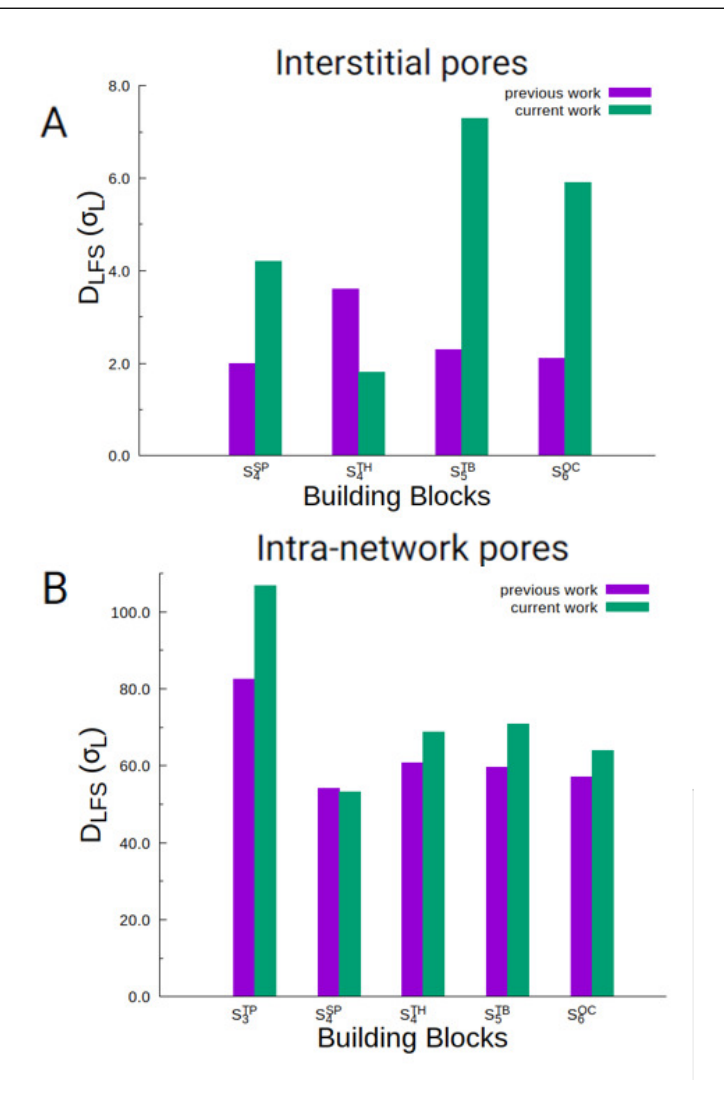


Figure 7. A comparison of interstitial pore diameters (panel A) and intra-network pore diameters (panel B), computed based on data from this study and our previous work on charged lobed particles [27]. Data are shown for only those particle types which form interstitial or intra-network pores in both studies. In Fig. S7, we also present pore diameters for self-assemblies of all particle types at all conditions from this study.

 S_4^{SP} particles where pores of similar size to our previous study [27] are observed. Overall, the intra-network pores are significantly larger than the interstitial pores. This is potentially relevant for applications of colloidal based systems in designing tissue engineering scaffolds in which interconnected larger pores are needed to allow cellular penetration and nutrient circulation [70]. The required sizes for the pores may vary according to the type of cells that are being targeted for growth in these scaffolds, but they typically range from ~ 30 -400 μ m for human cells [71]. Our simulations show that the lobed particles form interconnected networks with significantly larger pores compared to the particle-size which could be suitable for applications in designing tissue engineering scaffolds.

3.4 Particle Packing Modes: Interplanar Angles

To further probe the correlation between the porosity and the packing arrangements of particles within the self-assemblies, we computed the distributions of inter-planar angles between the planes $S-L^+-L^-$ and L^+-L^--S that are formed by the seed (S) and positively-charged as well as negatively-charged lobes (L^+/L^-) (Fig. 8). The inter-planar angle distributions for the S_2^{DB} (dumbbell) particles show the peaks near -180° and -180° (Fig. 8A). This indicates a linear or head-to-head arrangement of particles within the porous networks where the particles organize themselves in a parallel or an anti-parallel arrangement to form chain-like configurations (Fig. 4A). The angle distributions for the S_3^{TP} particles (Fig. 8B) show a broader range of inter-planar angle values spanned in self-assemblies of these particles. For example, a broader distribution of angle values exists in the range between -40° and -10°, while the distributions are sharply peaked at ~30° and ~180°. These observations can be attributed to the planar shapes of the S_3^{TP} particles which can arrange themselves in different modes including porous random aggregates (RA1, RA3; Fig. 3) and porous sheets with six-membered ring-like motifs (Fig. 5A).

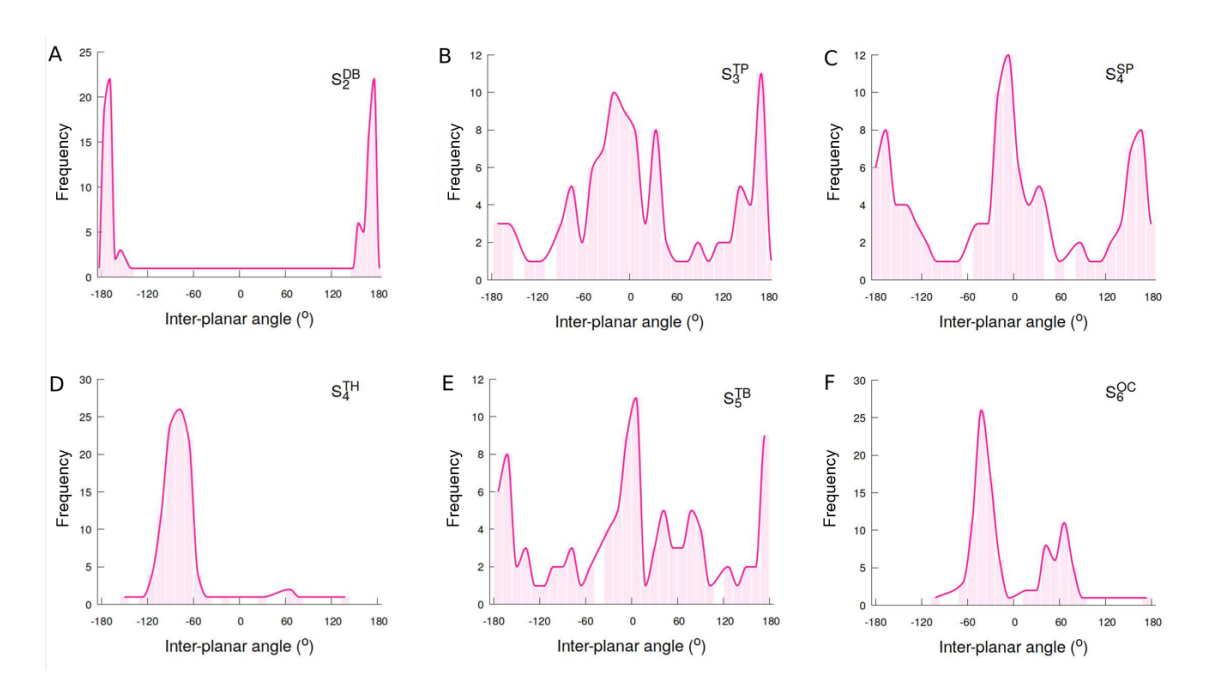


Figure 8. Shown are the distributions of inter-planar angles in self-assemblies formed by (A) dumbbell, (B) trigonal planar, (C) square planar, (D) tetrahedral, (E) trigonal bipyramidal, and (F) octahedral shaped particles.

The angle distributions for the S_4^{SP} particles are reported in Fig. 8C. These particles predominantly form sheet-like morphologies due to their planar structure. This feature is well captured from the interplanar angle distribution in which three peaks for the angle values -180°, 0°, 180° are observed. However, the non-planar S_4^{TH} particles having the same number of lobes do not form any planar morphologies which is also reflected in their interplanar angle distributions (Fig. 8D) showing that these particles align themselves

- by maintaining an angle of $\sim 90^{\circ}$. Therefore, due to their non-planarity, these particles break the parallel or anti-parallel alignment as found in the planar S_4^{SP} particles with the same number of lobes.
- The trigonal bipyramidal particles with five lobes (S_5^{TB}) show several different types of interplanar angles (Fig. 8E), similar to the S_3^{TP} particles. This can be attributed to the planar equatorial framework within the S_5^{TB} particles which resembles the S_3^{TP} geometry and also due to a higher number of lobes leading to different packing modes, which leads to the S_5^{TB} particles forming intra-network pores with the second largest sizes after the S_3^{TP} particles. Finally, the distributions of the S_6^{OC} particles are presented in Fig. 8F. These particles do not show a wider range of angle values as in the case of S_3^{TP} or S_5^{TB} particles. Instead,
- 286 the angle values are largely confined to \sim -40° or between \sim 40° and \sim 70°. The restricted arrangements for
- 287 these particles is attributed to the highest number of lobes to avoid several lobe-lobe replusions.

4 CONCLUSION

We studied self-assembly in the homogeneous mixtures of particles with oppositely-charged lobes and probed their pore forming tendencies. In these mixtures, each particle has all the lobes either positively-charged or negatively-charged to resemble functionalized lobed particles with complementary interactions that are potentially experimentally realizable in comparison to the particles where the lobes on the same particle have different charges [27]. We observed the formation of morphologies with interstitial as well as intra-network pores, where the pores in the latter morphologies are an order of magnitude larger than in the former morphologies. Among all the particles studied, the S_3^{TP} particles formed larger pores due to their smaller size, planar shape, and packing modes conducive to the formation of porous morphologies. We also observed that the mixtures of particles with oppositely-charged lobes have larger intra-network pores than the unmixed charged particles from our previous work [27]. Therefore, we suggest that the particle designs reported in our current work are suitable to applications in designing porous biomaterials for bioengineering and biomedical applications.

300

288

289

290

291

292

293

294

295

296

297

298

299

AUTHOR CONTRIBUTIONS

HV: conceptualization, supervision, funding acquisition, and draft editing. AS and BCR: modeling, simulation, analysis, and draft preparation. All authors contributed to the article and approved the submitted version.

FUNDING

- 304 We acknowledge the National Science Foundation (NSF) EPSCoR award (OIA-1757371; H.V.) for financial
- 305 support as well as for providing the hetereogenous CPU/GPU supercomputing facility at the University of
- 306 New Hampshire (UNH).

SUPPLEMENTAL MATERIAL

307 The supplemental data include 7 figures.

CONFLICT OF INTEREST STATEMENT

308 There are no conflicts to declare.

REFERENCES

- 309 [1] Whitesides GM, Grzybowski B. Self-assembly at all scales. Science 295 (2002) 2418–2421.
- 310 [2] Sacanna S, Pine DJ, Yi GR. Engineering shape: the novel geometries of colloidal self-assembly. *Soft*
- 311 *Matter* **9** (2013) 8096–8106.
- 312 [3] Matijevic E. Monodispersed metal (hydrous) oxides a fascinating field of colloid science. *Acc. Chem.*
- 313 Res. **14** (1981) 22–29.
- 314 [4] Matijevic E. Preparation and properties of uniform size colloids. *Chem. Mater.* **5** (1993) 412–426.
- 315 [5] Matijevic E. Uniform inorganic colloid dispersions. achievements and challenges. *Langmuir* 10
- 316 (1994) 8–16.
- 317 [6] Vold MJ. The effect of adsorption on the van der waals interaction of spherical colloidal particles. *J.*
- 318 *Colloid Sci.* **16** (1961) 1–12.
- 319 [7] Moncho-Jordá A, Martínez-López F, González AE, Hidalgo-Álvarez R. Role of long-range repulsive
- interactions in two-dimensional colloidal aggregation: experiments and simulations. *Langmuir* 18
- 321 (2002) 9183–9191.
- 322 [8] Min Y, Akbulut M, Kristiansen K, Golan Y, Israelachvili J. The role of interparticle and external
- forces in nanoparticle assembly. *Nat. Mater.* **7** (2008) 527–538.
- 324 [9] Lotito V, Zambelli T. Approaches to self-assembly of colloidal monolayers: A guide for
- nanotechnologists. Adv. Colloid Interface Sci. 246 (2017) 217–274.
- 326 [10] van Dommelen R, Fanzio P, Sasso L. Surface self-assembly of colloidal crystals for micro- and
- nano-patterning. Adv. Colloid Interface Sci. 251 (2018) 97–114.
- 328 [11] Lu PJ, Weitz DA. Colloidal particles: Crystals, glasses, and gels. Annu. Rev. Condens. Matter Phys 4
- 329 (2013) 217–233.
- 330 [12] Pham KN, Puertas AM, Bergenholtz J, Egelhaaf SU, Moussa
- id A, Pusey PN, et al. Multiple glassy states in a simple model system. Science **296** (2002) 104–106.

- 332 [13] Weeks ER, Crocker JC, Levitt AC, Schofield A, Weitz DA. Three-dimensional direct imaging of
- structural relaxation near the colloidal glass transition. *Science* **287** (2000) 627–631.
- 334 [14] Schall P, Cohen I, Weitz DA, Spaepen F. Visualization of dislocation dynamics in colloidal crystals.
- 335 Science **305** (2004) 1944–1948.
- 336 [15] Schall P, Cohen I, Weitz DA, Spaepen F. Visualizing dislocation nucleation by indenting colloidal
- 337 crystals. *Nature* **440** (2006) 319–323.
- 338 [16] Ghosh Chaudhuri R, Paria S. Core/shell nanoparticles: Classes, properties, synthesis mechanisms,
- characterization, and applications. *Chem. Rev.* **112** (2012) 2373–2433.
- 340 [17] Gao L, Gan H, Meng Z, Gu R, Wu Z, Zhang L, et al. Effects of genipin cross-linking of chitosan
- 341 hydrogels on cellular adhesion and viability. *Colloids Surf. B Biointerfaces* **117** (2014) 398–405.
- 342 [18] Gorai B, Rocha BC, Vashisth H. Design of Functionalized Lobed Particles for Porous Self-Assemblies.
- 343 *JOM-J. MIn. Met. Mat. S.* **73** (2021) 2413–2422.
- 344 [19] Ravaine S, Duguet E. Synthesis and assembly of patchy particles: Recent progress and future prospects.
- 345 *Curr. Opin. Colloid. Interface Sci.* **30** (2017) 45–53.
- 346 [20] Pawar AB, Kretzschmar I. Fabrication, assembly, and application of patchy particles. *Macromol*.
- 347 Rapid Commun. **31** (2010) 150–168.
- 348 [21] Bharti B, Rutkowski D, Han K, Kumar AU, Hall CK, Velev OD. Capillary bridging as a tool for
- assembling discrete clusters of patchy particles. J. Am. Chem. Soc. 138 (2016) 14948–14953.
- 350 [22] Long AW, Ferguson AL. Nonlinear machine learning of patchy colloid self-assembly pathways and
- mechanisms. J. Phys. Chem. B 118 (2014) 4228–4244.
- 352 [23] Zhang Z, Glotzer SC. Self-assembly of patchy particles. *Nano Lett.* **4** (2004) 1407–1413.
- 353 [24] Kraft DJ, Groenewold J, Kegel WK. Colloidal molecules with well-controlled bond angles. Soft
- 354 *Matter* **5** (2009) 3823.
- 355 [25] Paul S, Vashisth H. Self-assembly behavior of experimentally realizable lobed patchy particles. *Soft*
- 356 *Matter* **16** (2020) 8101–8107.
- 357 [26] Paul S, Vashisth H. Self-assembly of lobed particles into amorphous and crystalline porous structures.
- 358 *Soft Matter* **16** (2020) 1142–1147.
- 359 [27] Rocha BC, Paul S, Vashisth H. Enhanced porosity in self-assembled morphologies mediated by
- 360 charged lobes on patchy particles. *J. Phys. Chem. B* **125** (2021) 3208–3215.
- 361 [28] Blenner D, Stubbs J, Sundberg D. Multi-lobed composite polymer nanoparticles prepared by
- 362 conventional emulsion polymerization. *Polymer* **114** (2017) 54–63.
- 363 [29] Wang Y, Wang Y, Breed DR, Manoharan VN, Feng L, Hollingsworth AD, et al. Colloids with valence
- and specific directional bonding. *Nature* **491** (2012) 51–55.

- 365 [30] Liu M, Zheng X, Grebe V, He M, Pine DJ, Weck M. Two-dimensional (2d) or quasi-2d superstructures
- from DNA-coated colloidal particles. *Angew. Chem. Int. Ed.* **60** (2021) 5744–5748.
- 367 [31] van Ravensteijn BG, Kegel WK. Tuning particle geometry of chemically anisotropic dumbbell-shaped colloids. *J. Colloid Interface Sci.* **490** (2017) 462–477.
- 369 [32] Meester V, Verweij RW, van der Wel C, Kraft DJ. Colloidal recycling: Reconfiguration of random
- aggregates into patchy particles. ACS Nano 10 (2016) 4322–4329.
- 371 [33] Sacanna S, Pine DJ. Shape-anisotropic colloids: Building blocks for complex assemblies. Curr. Opin.
- 372 *Colloid Interface Sci.* **16** (2011) 96–105.
- 373 [34] Liu M, Dong F, Jackson NS, Ward MD, Weck M. Customized chiral colloids. J. Am. Chem. Soc. 142
- 374 (2020) 16528–16532.
- 375 [35] Liu M, Zheng X, Grebe V, Pine DJ, Weck M. Tunable assembly of hybrid colloids induced by
- regioselective depletion. *Nat. Mater.* **19** (2020) 1354–1361.
- 377 [36] Zheng X, Wang Y, Wang Y, Pine DJ, Weck M. Thermal regulation of colloidal materials architecture
- through orthogonal functionalizable patchy particles. *Chem. Mater.* **28** (2016) 3984–3989.
- 379 [37] Wolters JR, Avvisati G, Hagemans F, Vissers T, Kraft DJ, Dijkstra M, et al. Self-assembly of "mickey
- mouse" shaped colloids into tube-like structures: experiments and simulations. Soft Matter 11 (2015)
- 381 1067–1077.
- 382 [38] Kraft DJ, Vlug WS, van Kats CM, van Blaaderen A, Imhof A, Kegel WK. Self-assembly of colloids
- with liquid protrusions. J. Am. Chem. Soc. **131** (2008) 1182–1186.
- 384 [39] Morphew D, Shaw J, Avins C, Chakrabarti D. Programming hierarchical self-assembly of patchy
- particles into colloidal crystals via colloidal molecules. ACS Nano 12 (2018) 2355–2364.
- 386 [40] Avvisati G, Vissers T, Dijkstra M. Self-assembly of patchy colloidal dumbbells. J. Chem. Phys. 142
- 387 (2015) 084905.
- 388 [41] Wolters JR, Verweij JE, Avvisati G, Dijkstra M, Kegel WK. Depletion-induced encapsulation by
- dumbbell-shaped patchy colloids stabilize microspheres against aggregation. *Langmuir* **33** (2017)
- 390 3270–3280.
- 391 [42] Sato M. Effect of the interaction length on clusters formed by spherical one-patch particles on flat
- 392 planes. *Langmuir* **37** (2021) 4213–4221.
- 393 [43] Mathews K RA, Mani E. Stabilizing ordered structures with single patch inverse patchy colloids in
- two dimensions. *J. Condens. Matter Phys.* **33** (2021) 195101.
- 395 [44] Paul S, Vashisth H. Self-assembly of porous structures from a binary mixture of lobed patchy particles.
- 396 Front. Phys. 9 (2021) 767623.
- 397 [45] Wang Y, Wang Y, Breed DR, Manoharan VN, Feng L, Hollingsworth AD, et al. Colloids with valence
- and specific directional bonding. *Nature* **491** (2012) 51–55.

- 399 [46] Sacanna S, Korpics M, Rodriguez K, Colón-Meléndez L, Kim SH, Pine DJ, et al. Shaping colloids for
- 400 self-assembly. *Nat. Comm.* **4** (2013).
- 401 [47] Gong Z, Hueckel T, Yi GR, Sacanna S. Patchy particles made by colloidal fusion. *Nature* **550** (2017)
- 402 234–238.
- 403 [48] Meester V, Verweij RW, van der Wel C, Kraft DJ. Colloidal recycling: Reconfiguration of random
- aggregates into patchy particles. ACS Nano 10 (2016) 4322–4329.
- 405 [49] Lin YC, Tripathi AK, Tsavalas JG. Tunable multilobe particle geometry by annealing-assisted
- emulsion polymerization. ACS Appl. Polym. Mater. 4 (2022) 313–326.
- 407 [50] Glotzer SC, Solomon MJ, Kotov NA. Self-assembly: From nanoscale to microscale colloids. AIChE J.
- **50** (2004) 2978–2985. doi:10.1002/aic.10413.
- 409 [51] Marson RL, Phillips CL, Anderson JA, Glotzer SC. Phase behavior and complex crystal structures of
- self-assembled tethered nanoparticle telechelics. *Nano Lett.* **14** (2014) 2071–2078.
- 411 [52] Santos PHS, Campanella OH, Carignano MA. Brownian dynamics study of gel-forming colloidal
- 412 particles. J. Chem. Phys. B **114** (2010) 13052–13058.
- 413 [53] Santos PHS, Campanella OH, Carignano MA. Effective attractive range and viscoelasticity of colloidal
- gels. Soft Matter **9** (2013) 709–714.
- 415 [54] Chremos A, Jeong C, Douglas JF. Influence of polymer architectures on diffusion in unentangled
- 416 polymer melts. *Soft Matter* **13** (2017) 5778–5784.
- 417 [55] Liu T, VanSaders B, Keating JT, Glotzer SC, Solomon MJ. Effect of particles of irregular size on
- the microstructure and structural color of self-assembled colloidal crystals. *Langmuir* 37 (2021)
- 419 13300–13308.
- 420 [56] LeBard DN, Levine BG, Mertmann P, Barr SA, Jusufi A, Sanders S, et al. Self-assembly of coarse-
- grained ionic surfactants accelerated by graphics processing units. *Soft Matter* **8** (2012) 2385–2397.
- 422 [57] Anderson JA, Glaser J, Glotzer SC. Hoomd-blue: A python package for high-performance molecular
- dynamics and hard particle monte carlo simulations. *Comput. Mater. Sci.* **173** (2020) 109363.
- 424 [58] Hockney R, Goel S, Eastwood J. Quiet high-resolution computer models of a plasma. J. Comput.
- 425 *Phys.* **14** (1974) 148–158.
- 426 [59] LeBard DN, Levine BG, Mertmann P, Barr SA, Jusufi A, Sanders S, et al. Self-assembly of coarse-
- grained ionic surfactants accelerated by graphics processing units. *Soft Matter* **8** (2012) 2385–2397.
- 428 [60] Long AW, Ferguson AL. Nonlinear machine learning of patchy colloid self-assembly pathways and
- 429 mechanisms. J. Phys. Chem. B 118 (2014) 4228–4244.
- 430 [61] Ramasubramani V, Dice BD, Harper ES, Spellings MP, Anderson JA, Glotzer SC. freud: A software
- suite for high throughput analysis of particle simulation data. *Comput. Phys. Commun.* **254** (2020)
- 432 107275.

- 433 [62] Willems TF, Rycroft CH, Kazi M, Meza JC, Haranczyk M. Algorithms and tools for high-throughput
- geometry-based analysis of crystalline porous materials. *Micropor. Mesopor. Mat.* **149** (2012)
- 435 134–141.
- 436 [63] Pinheiro M, Martin RL, Rycroft CH, Jones A, Iglesia E, Haranczyk M. Characterization and
- comparison of pore landscapes in crystalline porous materials. J. Mol. Graph. Model. 44 (2013)
- 438 208–219.
- 439 [64] Pinheiro M, Martin RL, Rycroft CH, Haranczyk M. High accuracy geometric analysis of crystalline
- porous materials. *Cryst. Eng. Comm.* **15** (2013) 7531–7538.
- 441 [65] Zhang J, Luijten E, Granick S. Toward design rules of directional janus colloidal assembly. Annu. Rev.
- 442 *Phys. Chem.* **66** (2015) 581–600.
- 443 [66] Dias CS, Braga C, Araújo NAM, da Gama MMT. Relaxation dynamics of functionalized colloids on
- attractive substrates. *Soft Matter* **12** (2016) 1550–1557.
- 445 [67] Hagan MF, Elrad OM, Jack RL. Mechanisms of kinetic trapping in self-assembly and phase
- transformation. *J. Chem. Phys.* **135** (2011) 104115.
- 447 [68] Nykypanchuk D, Maye MM, van der Lelie D, Gang O. DNA-guided crystallization of colloidal
- nanoparticles. *Nature* **451** (2008) 549–552. doi:10.1038/nature06560.
- 449 [69] Paquet E, Viktor HL. Molecular dynamics, monte carlo simulations, and langevin dynamics: A
- 450 computational review. *BioMed Res. Int.* **2015** (2015) 1–18. doi:10.1155/2015/183918.
- 451 [70] O'brien FJ. Biomaterials & scaffolds for tissue engineering. *Materials today* **14** (2011) 88–95.
- 452 [71] Loh QL, Choong C. Three-dimensional scaffolds for tissue engineering applications: role of porosity
- 453 and pore size. *Tissue Eng.: Part B* **19** (2013) 485–502.